Effect of annealing conditions on the physio-chemical properties of spin-coated As_2Se_3 chalcogenide glass films

Yi Zou[1], Hongtao Lin[1], Okechukwu Ogbuu[1], Lan Li[1], Sylvain Danto[2], Spencer Novak[2], Jacklyn Wilkinson[2], J. David Musgraves[2], Kathleen Richardson[2], and Juejun Hu[1,*]

[1]Depatment of Materials Science & Engineering, University of Delaware, Newark, Delaware, 19716, USA
[2]The School of Materials Science and Engineering, COMSET, Clemson University, Clemson, South Carolina 29634, USA
** hujuejun@udel.edu*

Abstract: Thin film selenide glasses have emerged as an important material for integrated photonics due to its high refractive index, mid-IR transparency and high non-linear optical indices. We prepared high-quality As_2Se_3 glass films using spin coating from ethylenediamine solutions. The physio-chemical properties of the films are characterized as a function of annealing conditions. Compared to bulk glasses, as-deposited films possess a distinctively different network structure due to presence of Se-Se homo-polar bonds and residual solvent. Annealing partially recovers the As-Se_3 pyramid structure and brings the film refractive indices close to the bulk value. Optical loss in the films measured at 1550 nm wavelength is 9 dB/cm, which was attributed to N-H bond absorption from residual solvent.

OCIS codes: (160.2750) Glass and other amorphous materials; (310.3840) Materials and process characterization; (240.0310) Thin films; (310.1860) Deposition and fabrication; (230.7370) Waveguides;

References and links

1. A. Zakery and S. R. Elliott, "Optical properties and applications of chalcogenide glasses: a review," J. Non-Cryst. Solids **330**, 1-12 (2003).
2. J. S. Sanghera and I. D. Aggarwal, "Active and passive chalcogenide glass optical fibers for IR applications: a review," J. Non-Cryst. Solids **257**, 6-16 (1999).
3. M. Asobe, "Nonlinear optical properties of chalcogenide glass fibers and their application to all-optical switching," Opt. Fiber Technol. **3**, 142-148 (1997).
4. K. Tanaka, "Optical nonlinearity in photonic glasses," J. Mater. Sci.-Mater. Electron. **16**, 633-643 (2005).
5. P. Lucas, "Energy landscape and photoinduced structural changes in chalcogenide glasses," J. Phys.-Condes. Matter **18**, 5629-5638 (2006).
6. L. Petit, N. Carlie, T. Anderson, J. Choi, M. Richardson, and K. C. Richardson, "Progress on the Photoresponse of Chalcogenide Glasses and Films to Near-Infrared Femtosecond Laser Irradiation: A Review," IEEE J. Sel. Top. Quantum Electron. **14**, 1323-1334 (2008).
7. J. J. Hu, "Ultra-sensitive chemical vapor detection using micro-cavity photothermal spectroscopy," Opt. Express **18**, 22174-22186 (2010).
8. H. T. Lin, Z. Yi, and J. J. Hu, "Double resonance 1-D photonic crystal cavities for single-molecule mid-infrared photothermal spectroscopy: theory and design," Opt. Lett. **37**, 1304-1306 (2012).
9. J. J. Hu, V. Tarasov, N. Carlie, N. N. Feng, L. Petit, A. Agarwal, K. Richardson, and L. Kimerling, "Si-CMOS-compatible lift-off fabrication of low-loss planar chalcogenide waveguides," Opt. Express **15**, 11798-11807 (2007).
10. V. I. Mikla and V. V. Mikla, "Effect of thermal evaporation conditions on structural changes in amorphous As_xS_{1-x} films," Optoelectron. Adv. Mater.-Rapid Commun. **1**, 272-276 (2007).
11. V. Nazabal, F. Charpentier, J. L. Adam, P. Nemec, H. Lhermite, M. L. Brandily-Anne, J. Charrier, J. P. Guin, and A. Moreac, "Sputtering and Pulsed Laser Deposition for Near- and Mid-Infrared Applications: A

Comparative Study of $Ge_{25}Sb_{10}S_{65}$ and $Ge_{25}Sb_{10}Se_{65}$ Amorphous Thin Films," Int. J. Appl. Ceram. Technol. **8**, 990-1000 (2011).

12. M. Krbal, T. Wagner, T. Kohoutek, P. Nemec, J. Orava, and M. Frumar, "The comparison of Ag-$As_{33}S_{67}$ films prepared by thermal evaporation (TE), spin-coating (SC) and a pulsed laser deposition (PLD)," J. Phys. Chem. Solids **68**, 953-957 (2007).
13. M. Erazu, J. Rocca, M. Fontana, A. Urena, B. Arcondo, and A. Pradel, "Raman spectroscopy of chalcogenide thin films prepared by PLD," J. Alloys Compd. **495**, 642-645 (2010).
14. J. D. Musgraves, N. Carlie, J. Hu, L. Petit, A. Agarwal, L. C. Kimerling, and K. A. Richardson, "Comparison of the optical, thermal and structural properties of Ge-Sb-S thin films deposited using thermal evaporation and pulsed laser deposition techniques," Acta Mater. **59**, 5032-5039 (2011).
15. G. C. Chern and I. Lauks, "Spin-coated amorphous-chalcogenide films," J. Appl. Phys. **53**, 6979-6982 (1982).
16. T. Kohoutek, T. Wagner, J. Orava, M. Krbal, A. Fejfar, T. Mates, S. O. Kasap, and M. Frumar, "Surface morphology of spin-coated As-S-Se chalcogenide thin films," J. Non-Cryst. Solids **353**, 1437-1440 (2007).
17. S. S. Song, N. Carlie, J. Boudies, L. Petit, K. Richardson, and C. B. Arnold, "Spin-coating of $Ge_{23}Sb_7S_{70}$ chalcogenide glass thin films," J. Non-Cryst. Solids **355**, 2272-2278 (2009).
18. C. Tsay, Y. L. Zha, and C. B. Arnold, "Solution-processed chalcogenide glass for integrated single-mode mid-infrared waveguides," Opt. Express **18**, 26744-26753 (2010).
19. C. Tsay, F. Toor, C. F. Gmachl, and C. B. Arnold, "Chalcogenide glass waveguides integrated with quantum cascade lasers for on-chip mid-IR photonic circuits," Opt. Lett. **35**, 3324-3326 (2010).
20. T. Kohoutek, T. Wagher, M. Vlcek, and M. Frumar, "Physico-chemical properties of spin-coated Ag-As-Sb-S films," J. Non-Cryst. Solids **351**, 2205-2209 (2005).
21. T. Kohoutek, T. Wagner, M. Frumar, A. Chrissanthopoulos, O. Kostadinova, and S. N. Yannopoulos, "Effect of cluster size of chalcogenide glass nanocolloidal solutions on the surface morphology of spin-coated amorphous films," J. Appl. Phys. **103**, 063511 (2008).
22. T. Kohoutek, T. Wagner, J. Orava, M. Frumar, V. Perina, A. Mackova, V. Hnatowitz, M. Vlcek, and S. Kasap, "Amorphous films of Ag-As-S system prepared by spin-coating technique, preparation techniques and films physico-chemical properties," Vacuum **76**, 191-194 (2004).
23. S. S. Song, J. Dua, and C. B. Arnold, "Influence of annealing conditions on the optical and structural properties of spin-coated As_2S_3 chalcogenide glass thin films," Opt. Express **18**, 5472-5480 (2010).
24. T. Kohoutek, T. Wagner, M. Vlcek, and M. Frumar, "Spin-coated $As_{33}S_{67-x}Se_x$ thin films: the effect of annealing on structure and optical properties," J. Non-Cryst. Solids **352**, 1563-1566 (2006).
25. S. Shtutina, M. Klebanov, V. Lyubin, S. Rosenwaks, and V. Volterra, "Photoinduced Phenomena in spin-coated vitreous As_2S_3 and AsSe films," Thin Solid Films **261**, 263-265 (1995).
26. T. Guiton and C. Pantano, "Solution/gelation of arsenic trisulfide in amine solvents," Chem. Mater. **1**, 558-563 (1989).
27. M. A. Popescu, *Non-Crystalline Chalcogenicides* (Kluwer Academic Publishers, Dordrecht, Netherlands, 2001).
28. M. Waldmann, J. D. Musgraves, K. Richardson, and C. B. Arnold, "Structural properties of solution processed $Ge_{23}Sb_7S_{70}$ glass materials," J. Mater. Chem. (to be published).
29. R. J. Nemanich, G. A. N. Connell, T. M. Hayes, and R. A. Street, "Thermally induced effects in evaporated chalcogenide films. 1. structure," Phys. Rev. B **18**, 6900-6914 (1978).
30. J. J. Hu, V. Tarasov, N. Carlie, L. Petit, A. Agarwal, K. Richardson, and L. Kimerling, "Exploration of waveguide fabrication from thermally evaporated Ge-Sb-S glass films," Opt. Mater. **30**, 1560-1566 (2008).
31. W. Y. Li, S. Seal, C. Rivero, C. Lopez, K. Richardson, A. Pope, A. Schulte, S. Myneni, H. Jain, K. Antoine, and A. C. Miller, "Role of S/Se ratio in chemical bonding of As-S-Se glasses investigated by Raman, x-ray photoelectron, and extended x-ray absorption fine structure spectroscopies," J. Appl. Phys. **98**, 053503 (2005).
32. V. Kovanda, M. Vlcek, and H. Jain, "Structure of As-Se and As-P-Se glasses studied by Raman spectroscopy," J. Non-Cryst. Solids **326**, 88-92 (2003).
33. NIST, "Ethylenediamine", retrieved 7/15/2012, http://webbook.nist.gov/cgi/cbook.cgi?Name=ethylenediamine&Units=SI.
34. R. Swanepoel, "Determination of the thickness and optical-constants of amorphous-silicon," J. Phys. E. Sci. Instrum. **16**, 1214-1222 (1983).
35. N. Carlie, N. C. Anheier, H. A. Qiao, B. Bernacki, M. C. Phillips, L. Petit, J. D. Musgraves, and K. Richardson, "Measurement of the refractive index dispersion of As_2Se_3 bulk glass and thin films prior to and after laser irradiation and annealing using prism coupling in the near- and mid-infrared spectral range," Rev. Sci. Instrum. **82**, 053103 (2011).
36. R. P. Wang, S. J. Madden, C. J. Zha, A. V. Rode, and B. Luther-Davies, "Annealing induced phase transformations in amorphous As_2S_3 films," J. Appl. Phys. **100**, 063524 (2006).
37. C. Tsay, E. Mujagic, C. K. Madsen, C. F. Gmachl, and C. B. Arnold, "Mid-infrared characterization of solution-processed As_2S_3 chalcogenide glass waveguides," Opt. Express **18**, 15523-15530 (2010).

1. Introduction

Chalcogenide glasses are ideal candidates for various applications in photonic systems because of their wide transparency window from the visible to mid-IR region [1, 2], high optical nonlinearities [3, 4], photosensitivity [5, 6], and large photothermal figure-of-merit [7, 8]. Chalcogenide glass films are most commonly deposited either by thermal evaporation [9, 10], sputtering [11], or pulsed laser deposition [12-14]. Amine solution processing, first developed in the 1980s [15-17], has recently emerged as a promising technique for low-cost, large-area chalcogenide glass film deposition. In addition, it has been shown that solution processing can be combined with soft lithography such as micro-molding in capillaries [18] and micro-transfer molding [19] for photonic device fabrication.

Previous efforts on chalcogenide glass films via spin-coating have mostly focused on sulfides [12, 15, 17, 20-23]; solution processing of selenide glasses, on the other hand, is much less explored [15, 24, 25]. Difficulties in dissolving selenides partly account for this lack of research coverage. While we observed poor selenide solubility in propylamine and butylamine (solvents widely used in sulfide spin-coating), ethylenediamine (EDA) serves as a good solvent for selenide glasses. Previous studies by Guiton *et al.* suggest that the As_2S_3 chalcogenide dissolution process in EDA proceeds as the EDA molecules chelate between As atoms, which breaks the As_2S_3 pyramid network and forms EDA chelated As_4S_4 units interconnected by S-S homopolar bonds [26]. Given the structural resemblance between As_2S_3 and As_2Se_3 (both types of glasses consist of As-chalcogen trigonal pyramids [27], it is reasonable to postulate a similar chelation dissolution mechanism of As_2Se_3 glass in EDA. To validate this model, the structural and optical properties of spin-coated As_2Se_3 films were evaluated in this study. Finally, as a proof-of-concept device application, optical guiding in planar waveguides in spin-coated As_2Se_3 films was also demonstrated.

2. Film deposition and morphology

Solutions of As_2Se_3 were prepared by dissolving As_2Se_3 powder (Alfa Aesar Inc., 99.999%) into ethylenediamine (Fluka Chemicals, $\geq$ 99.5%). The dissolution process was carried out inside a sealed glass container to prevent solvent evaporation. A hot plate with magnetic stirrer was used to expedite the dissolution process. The solution was then centrifuged at a rate of 4000 rpm for 10 min and filtered using syringe filter with 0.2 micron filtration membrane to remove suspended particles and insoluble impurities. A maximum glass loading of 0.6 g/mL in EDA was achieved without apparent phase separation or precipitation in the solution. The resulting solution was stored inside a nitrogen-purged glove box until use to prevent oxygen and water contamination. During spin-coating, 1.5 milliliters of solution with desired concentrations of As_2Se_3 was pipetted onto a substrate (microscope slides from Fisher Scientific Inc. or 3" silicon wafer from Silicon Quest International), and spun at various rates for 30 s. The resulting films are pre-baked in a nitrogen atmosphere at 60 °C for 30 min immediately after spin coating. In the present study, we chose films deposited from solutions with 0.2 g/mL glass loading at a spin speed of 1000 rpm to evaluate the impact of annealing on film structure and properties. Thickness of these as-deposited films was measured to be (428 ± 8) nm using a Dektak II surface profilometer. The amorphous nature of all films used in this study was confirmed by X-ray diffraction.

The as-deposited films were annealed in an ambient environment as well as in vacuum. Films annealed in an ambient environment were dotted with self-assembled arsenic oxide crystals on the surface. As is shown in the scanning electron microscope (SEM) image in Fig. 1, most of these crystals are 1 to 5 microns in size, and exhibit a nearly perfect triangular shape. Their composition was measured using energy dispersive X-ray spectroscopy (EDX) to be AsO_x (atomic ratio) where x varies from 2 to 2.8 (Table 1).

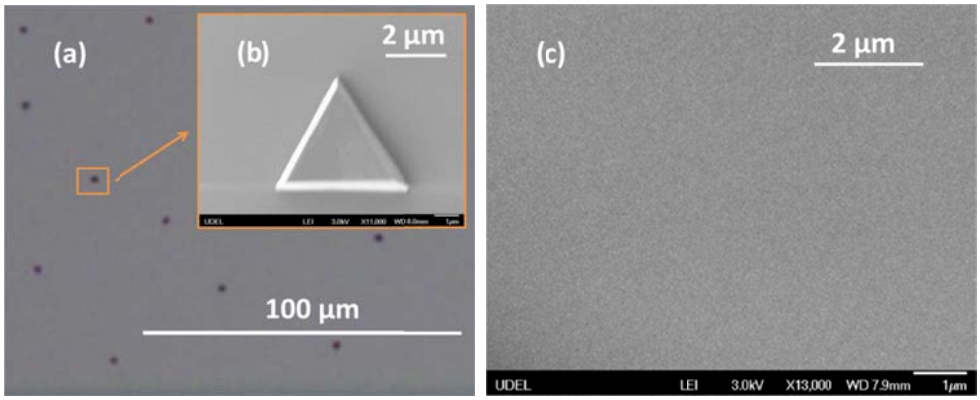

Fig. 1. Top-view images of spin-coated As_2Se_3 films: (a) optical micro graph of the as-deposited As_2Se_3 films annealed in the ambient atmosphere (b) SEM image of a self-assembled AsO_x crystal formed on films annealed in the ambient atmosphere; (c) films annealed in vacuum showing a smooth, featureless surface.

In contrast, films annealed in vacuum show a smooth, featureless surface finish under SEM examination. Since photonic device applications generally require smooth film surfaces with low roughness, results presented henceforth in the paper are based on films annealed in vacuum. We chose a maximum vacuum annealing temperature of 170 °C, above which partial evaporation of As_2Se_3 occurred. According to our EDX measurement, composition of the films annealed in vacuum showed < 1% deviation from bulk stoichiometry (Table 1).

Table 1. EDX composition analysis of spin-coated As_2Se_3 films annealed in non-oxygen and oxygen-containing environment

	Film compositions (atom %, averaged over measurements at 4 points)			
	As (atom %)	Se (atom %)	O (atom %)	
Vacuum annealed As_2Se_3 films	39.7	60.3	0	As/Se = 0.66 ± 0.03
Self-assembled AsO_x particles	29.4	0	70.6	As:O = 0.42 ± 0.08

Surface roughness of as-deposited and annealed films was measured through atomic force microscopy (AFM) on a Dimension 3100 (Digital Instruments, Inc.) microscope. Silicon AFM probes (Tap 150-G from Budget Sensors, Inc) with a force constant of 5 N/m and a resonant frequency of 150 KHz were used. Fig. 2a plots the film thickness and RMS surface roughness as a function of annealing conditions. Both film thickness and surface roughness are reduced as the annealing temperature and time increase. Fig. 2b-2h shows the surface morphology evolution during annealing. The surface of as-deposited film is covered by bubble-like nanostructures with an average diameter of ~ 100 nm. We hypothesize that these circular structures are solvent micelles formed during spin-coating and the pre-baking step. During annealing, residual solvent trapped in the micelles evaporates. Such micelle shrinkage leads to film densification and consequently film thickness and roughness reduction. Notably, a nanoporous micro-structure was observed in spin-coated $Ge_{23}Sb_7S_{70}$ films, which was believed to be originated from removal of trapped n-propylamine solvent [28]. However, in our case the annealing process was able to completely remove the micelles and produce dense As_2Se_3 films. No nanopore formation was observed as is shown in Fig. 3.

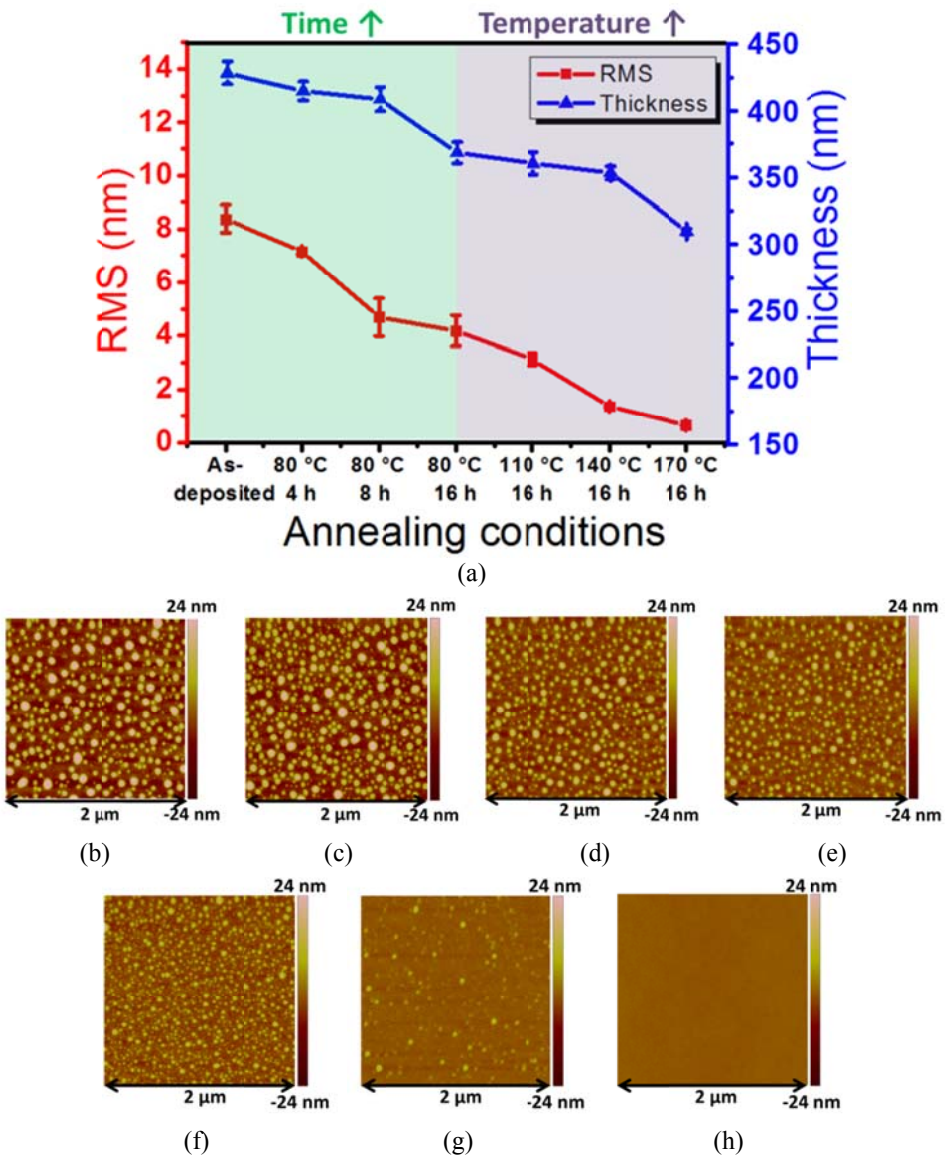

Fig. 2. (a) Thickness and surface roughness of spin coated As_2Se_3 glass films annealed at different conditions. (b)-(h) AFM surface profiles (2µm × 2µm) of glass films annealed at various conditions: (b) as-deposited film; (c) film annealed at 80 °C for 4 hours; (d) film annealed at 80 °C for 8 hours; (e) film annealed at 80 °C for 16 hours; (f) film annealed at 110 °C for 16 hours; (g) film annealed at 140 °C for 16 hours; (h) film annealed at 170 °C for 16 hours.

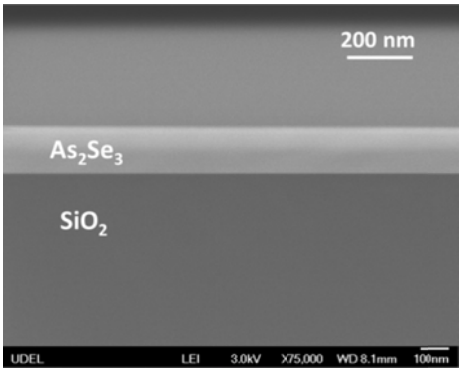

Fig. 3. Cross-sectional SEM image of spin-coated As_2Se_3 films after annealing. Annealing leads to a dense, defect-free film microstructure.

3. Structural analysis using micro-Raman spectroscopy

Raman spectroscopy has been proven to be a powerful tool for glass structure identification [29]. The micro-Raman spectra for the parent bulk glass and deposited films were recorded using a Bruker Senterra Raman spectrometer with a Raman microprobe attachment. This system has a typical resolution of 2-3 cm^{-1} at room temperature and uses a backscattering geometry. The system consists of an edge filter for Rayleigh rejection, a microscope equipped with × 10, × 50 and × 100 objectives and a CCD detector. A 785 nm NIR semiconductor laser was used for excitation with an incident power of approximately 2 mW. The use of a 785 nm source with a low power was specific to our study in order to avoid any photo-structural changes which the laser beam might induce in the samples during measurement. Three measurements per sample were compared and averaged, and the resulting spectra were illustrated in Fig. 4a.

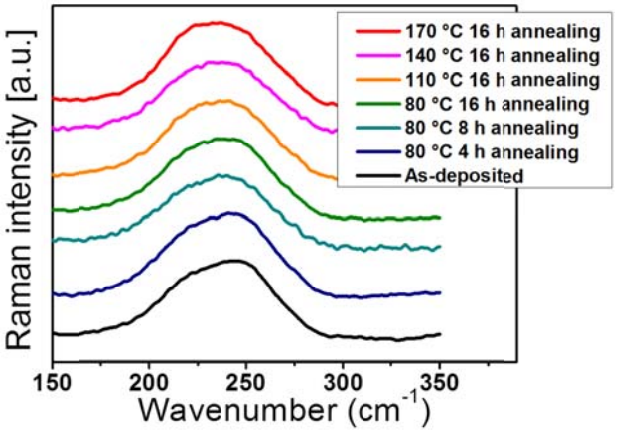

(a)

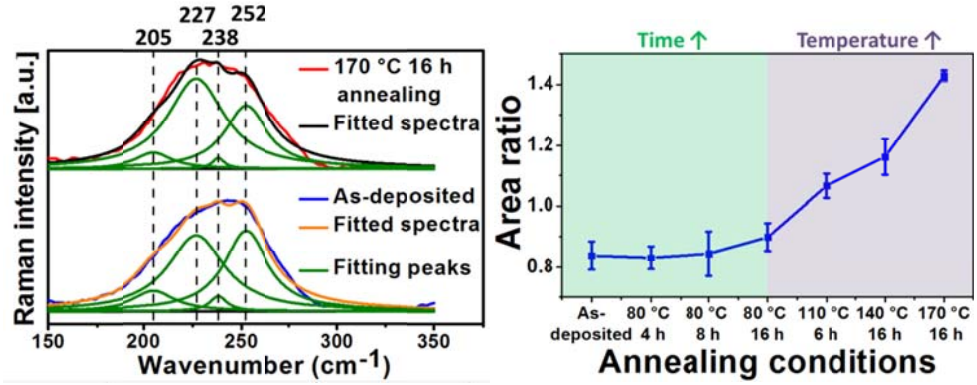

(b) (c)

Fig.4 (a) Raman spectra of spin coated As_2Se_3 films under different annealing conditions; the spectra are vertically offset for clarity; (b) Raman spectra from an as-deposited film and a film annealed at 170 °C for 16 hours were fitted by keeping the position of the peaks constant; (c) The peak area ratio, as determined by the area of $AsSe_3$ pyramidal unit peaks over the area of peaks corresponding to As_4Se_4 unit, Se-Se chain and Se-Se ring, as a function of annealing conditions.

Table 2 Raman peak position and peak assignments

Peak Position (Wave number, cm^{-1})	Peak assignment
205	As_4Se_4 unit
227	$AsSe_3$ pyramid unit
238	Se-Se chain
252	Se-Se ring

The dominant features in the glass Raman spectra are the broad bands located at 200 – 300 cm^{-1}. The broad band can be further deconvoluted into four peaks, each corresponds to a distinctive vibrational mode belonging to a specific structural group. In order to understand the structure variation, the spectra were fitted keeping the position of the peaks constant [30, 31]. Fig. 4b illustrates two examples of the fitting result for as-deposited film and a film annealed at 170 °C for 16 hours. According to Li *et al.* [32], peaks located at 205 cm^{-1}, 227 cm^{-1}, 238 cm^{-1} and 252 cm^{-1} are assigned to the vibrational modes of As_4Se_4 units, $AsSe_3$ pyramidal units, Se-Se chain and Se-Se ring respectively (Table 2). The As_4Se_4 units, Se-Se chain and ring units contain homopolar bonds which are only formed during the EDA chelation process and are absent in bulk As_2Se_3 glass. This observation is consistent with the proposed dissolution mechanism [26]: solution deposition from EDA-As_2Se_3 solution essentially involves As-Se heteropolar bond breaking and new Se-Se homopolar bond formation. Since the $AsSe_3$ pyramids represent the dominant structural unit in bulk glasses and the Se-Se homopolar bonds originated from the solvent chelation process, we plot the peak area ratio, the area of $AsSe_3$ pyramidal unit peaks over the area of peaks corresponding to As_4Se_4 unit, Se-Se chain and Se-Se ring, as a function of annealing conditions in Fig. 4c. With increasing of annealing time and temperature, the peak area ratio monotonically increases, which indicates that the re-polymerization process accompanying annealing brings spin coated films close to the structure of bulk glasses.

4. Optical property characterizations

We used infrared spectroscopy to monitor EDA solvent removal in annealed films. Infrared transmission spectra of the films were measured with a Perkin-Elmer Spectrum 100 series

spectrometer with a Universal diamond ATR attachment. Fig. 5a shows the absorption spectra of as-deposited and annealed spin-coated films. Spectrum collected on a thermally evaporated As_2Se_3 film is also included for comparison. We observed a remarkable decrease of N-H stretching modes at 1580, 3140 and 3310 cm^{-1} as the annealing time or temperature increases. The double absorption peaks located at 2860 and 2940 cm^{-1} and peaks around 1455 cm^{-1} are attributed to C-H bonds associated with the amine molecules. All these spectral features are absent in the spectrum collected on the EDA-free, thermally evaporated film. Peak absorbance values for peaks at 1580, 3140 and 3310 cm^{-1} as a function of annealing conditions are plotted in Fig. 5b. Apparently, annealing at higher temperature or longer time leads to diminishing infrared absorption, indicating effective removal of organic solvent in the films. However, persistent presence of the absorption peaks makes it clear that there is still residual solvent left in the films annealed in vacuum at the maximum temperature of 170 °C for 16 hours. This is a somewhat surprising result given the much lower boiling point of EDA in an ambient environment (118 °C [33]). To explain this phenomenon, we again refer to the Guiton's model which suggests the formation of EDA-As_2Se_3 chelated molecules upon glass dissolution. Chelation increases the bonding affinity between EDA and selenides, which impedes solvent removal during annealing. Parasitic infrared optical absorption in the spin-coated films due to the residual solvent was quantified using waveguide measurement and the results are summarized in section 5.

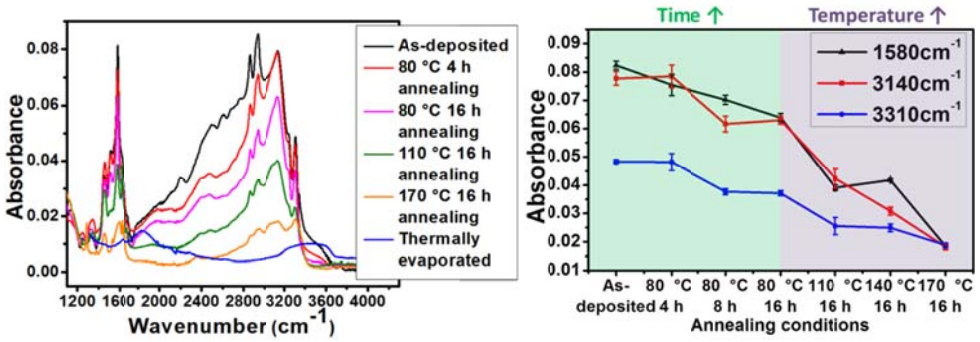

(a) (b)

Fig.5 (a) FTIR absorption spectra of EDA-derived As_2Se_3 films vacuum annealed at conditions. (b) Peak absorbance at 1580, 3140 and 3310 cm^{-1} (due to N-H stretching modes) of EDA-derived As_2Se_3 films. The decrease of peak absorbance indicates progressive solvent removal during annealing.

A Perkin-Elmer 1050 UV-Vis spectrophotometer is used to record the transmittance spectra of glass films in the range of 450-2000 nm. The film refractive indices were calculated from the transmittance spectra using the Swanepoel's method [34]. The transmittance spectra and fitted refractive index values at 1500 nm wavelength are plotted in Fig. 6a and 6b, respectively. As-deposited film shows a low refractive index of 2.44, much lower than the corresponding bulk value of 2.83 [35]. After annealing at 170 °C for 16 hours, the As-Se_3 pyramid structure units are partially restored and the residual solvent is mostly removed, and the film index thus becomes 2.74, approaching the bulk value at 1500 nm wavelength. The partial recovery of film refractive index to its corresponding bulk value was observed in thermally evaporated chalcogenide glass films as well [35, 36].

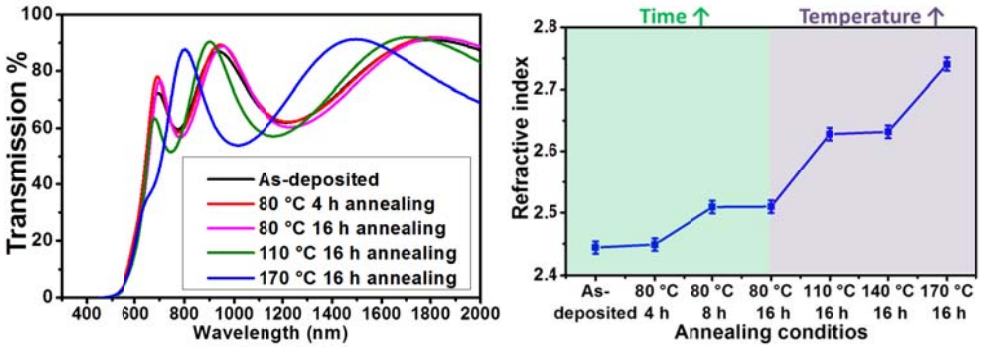

(a) (b)

Fig 7. (a) UV-Vis transmission spectra of spin-coated As_2Se_3 films from EDA solution with different annealing conditions. The spectra are not corrected for Fresnel reflection. (b) Effect of annealing on film refractive indices measured at 1500 nm wavelength.

5. Waveguide fabrication and optical loss measurement at 1550 nm wavelength

Since N-H bonds exhibit an infrared absorption overtone near 1500 nm wavelength, it is expected that the residual solvent in spin-coated films can pose additional optical loss at the 1550 nm telecommunication wave band. To validate the optical performance of the spin-coated films, we fabricated planar inverted ridge waveguides using a process flow schematically shown in Fig 7. A photoresist pattern is first defined on an oxide-coated Si wafer using photolithography, followed by a Buffered Oxide Etch (BOE) to define trenches in the silica cladding layer. After removal of the photoresist, an As_2Se_3 glass layer is spin coated and vacuum annealed at 140 °C for 16 hours to complete the inverted ridge waveguide structure fabrication.

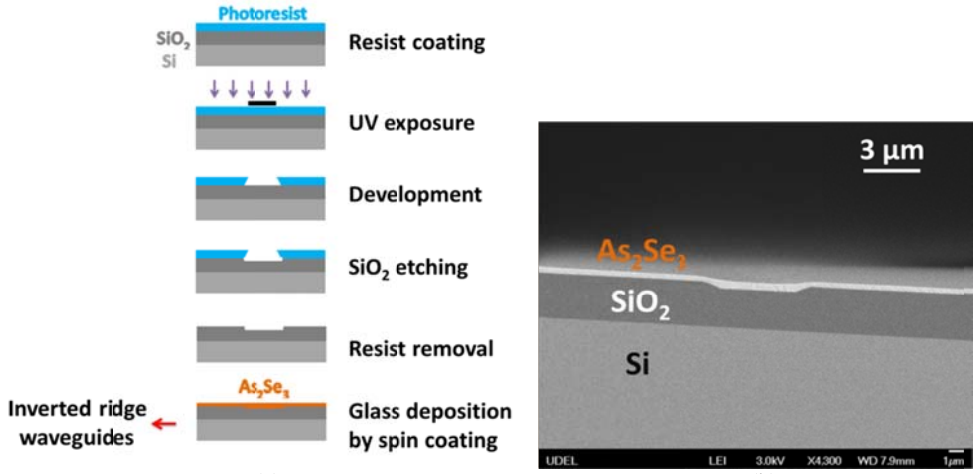

(a) (b)

Fig. 7. (a) Schematic process flow of As_2Se_3 inverted ridge waveguides. (b) a cross-sectional SEM image of an inverted ridge waveguide from spin coated As_2Se_3 glass

Optical loss in the waveguides is measured using a fiber end-fire coupling method and the cut-back technique, and is 9 dB/cm at 1550 nm wavelength, as shown in Fig 8. This loss figure is comparable to previously reported values measured in solution processed sulfide glass waveguides [37]; however, it is much higher compared to the loss in rib waveguides fabricated in thermally evaporated chalcogenide glass films (< 1 dB/cm). The optical loss is almost independent of the waveguide widths, indicating that sidewall roughness scattering is

insignificant in the devices. We thus attribute the additional loss to N-H bond overtone absorption caused by residual solvent in the films.

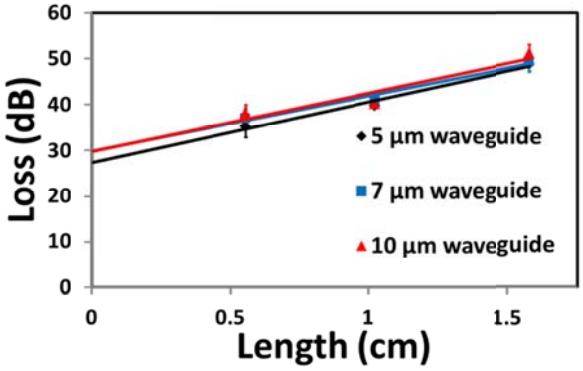

Fig. 8 Total insertion loss of the As_2Se_3 waveguides plotted as a function of wavelength lengths. The slopes of the curves yield the propagation loss in the waveguides, while the intercepts with the vertical axis give the coupling loss. The three curves correspond to waveguides of three different widths.

5. Conclusions

In this report, we demonstrate the successful deposition of stoichiometric As_2Se_3 films using a solution-based spin-coating technique. The influence of annealing conditions on physiochemical properties of spin coated films was evaluated in detail through structure, morphology and optical property characterizations. As-deposited films are structurally dissimilar to bulk glasses in that they contain a large fraction of Se-Se homopolar bonds and residual solvents, which is consistent with the EDA chelation dissolution model proposed for film formation from solution. The increase of annealing time and temperature leads to solvent molecule removal from the chelated sites as well as a structural transformation towards the "bulk state" characterized by dominating As-Se_3 pyramidal units. Annealing process also leads to condensed films with very low surface roughness (< 1 nm RMS) and increases the refractive index from 2.45 (as-deposited) to 2.75 (annealed at 170 °C for 16 h), which is close to the bulk value of 2.83 at 1550 nm wavelength. Unlike spin-coated $Ge_{23}Sb_7S_{70}$ glass, we did not observe nanopore formation in the annealed As_2Se_3 films. As a proof-of-concept integrated photonic device, inverted ridge waveguides are fabricated using spin-coating and a propagation loss of 9 dB/cm was measured using cut-back. This relatively high loss value is attributed to N-H overtone absorption by residual solvent. Understanding of physiochemical properties in the spin-coated As_2Se_3 glass films paves the pathway for potential new applications in integrated photonics.

Acknowledgments

The authors would like to thank funding support provided by the Department of Energy under award number DE-EE0005327 and the University of Delaware Research Foundation (UDRF). Clemson co-authors acknowledge funding provided in part by the US Department of Energy [Contract # DE- NA000421], NNSA/DNN R&D. This paper has been prepared as an account of work partially supported by an agency of the United States Government. Neither the United States Government nor any agency thereof, nor any of their employees, makes any warranty, express or implied, or assumes any legal liability or responsibility for the accuracy, completeness or usefulness of any information, apparatus, product or process disclosed, or represents that its use would not infringe privately owned rights. Reference herein to any